CHINESE OPTICS LETTERS

Vol. 19, No. 11 | November 2021

Mid-infrared flat-topped broadband chiral helix metamaterials based on indium tin oxide and their chiral properties

Wentao Zhang (张文涛)[1], Weijie Shi (施维捷)[2], Hui Guo (郭 慧)[2], and Changchun Yan (闫长春)[2*]

[1] School of Physics and New Energy, Xuzhou Institute of Technology, Xuzhou 221018, China

[2] Jiangsu Key Laboratory of Advanced Laser Materials and Devices, School of Physics and Electronic Engineering, Jiangsu Normal University, Xuzhou 221116, China

*Corresponding author: yancc@jsnu.edu.cn

Received February 13, 2021 | Accepted April 15, 2021 | Posted Online August 23, 2021

We proposed a periodic mid-infrared broadband chiral structure. Its unit cell consists of four indium tin oxide (ITO) helix subunits with different radii. The simulation results show that the flat-topped broadband circular dichroism (CD) can be achieved in the mid-infrared band by optimizing the parameters of helix structures. The simulation results also show that compared with the metallic (Ag and Au) helix structures, the ITO helix structure proposed exhibits evidently better broadband CD and optical activity, which provides a new idea for the design of broadband polarization state control devices in the mid-infrared band.

Keywords: mid-infrared; flat-topped broadband; chiral helix metamaterial.

DOI: 10.3788/COL202119.111601

1. Introduction

New materials and technologies, such as metamaterials[1–3], plasmonics[4–6], graphene[7–9], metasurface[10,11], and nanomaterials[12,13], are constantly emerging in order to manipulate electromagnetic waves and make new progress. Mid-infrared lasers have important applications in communications and medical treatments. The effective transmission control of polarization states on the mid-infrared lasers is an important factor, which is indispensable for their better applications. Chiral metamaterials, a new kind of artificial electromagnetic materials, have been intensively studied and show strong abilities in polarization state controls[14–21]. Such abilities generally only occur near the oscillation wavelengths of the metamaterials. At present, the proven responses of the chiral metamaterials are mainly distributed in the microwave[22], terahertz[23], visible, or near-infrared regions[24–32]. Only a few researchers reported the responses distributing in the mid-infrared band[33–36]. In these works, the conventional metals such as copper, silver (Ag), and gold (Au) were used as plasmonic materials. The metal materials have large real parts of permittivities, low chemical stability, and poor compatibility with the standard silicon manufacturing processes. These shortcomings affect the polarization control performances of the mid-infrared chiral metamaterials composed of conventional metals. Metal oxides[37] were found to be good alternative plasmonic materials in the mid-infrared band due to their low losses. Our group previously selected indium tin oxide (ITO) as a plasmonic material to fabricate an L-shaped mid-infrared chiral structure[36]. The structure exhibited circular dichroism (CD) responses stronger than those of the structure consisting of Ag in the mid-infrared band.

In this paper, ITO is selected to design a periodic helix structure. Each helix unit cell consists of four helices with different radii. The simulation results show that the structure has flat-topped broadband CD, which is unattainable for the Au or Ag helix structures.

2. Structure Design

A periodic helix array structure was designed in this paper. Each unit cell consists of four subunits, each of which is composed of a helix, and the different helices have different radii, as shown in Fig. 1. The helix radii of the four subunits are $R_1 = 0.3\,\mu m$, $R_2 = 0.35\,\mu m$, $R_3 = 0.4\,\mu m$, and $R_4 = 0.45\,\mu m$, respectively. The materials of the helix and substrate are set to ITO and silicon, respectively. The radius of the wire is $r = 0.2\,\mu m$, the pitch of the helix is $p = 1\,\mu m$, the number of helix turns is $N = 1$, and the period of the unit cell is $a = 3.4\,\mu m$. The coordinate origin is located on the upper surface of the substrate and set at the center of the unit cell. Each subunit is located in the middle of every quarter unit cell. The helix structure we proposed can be

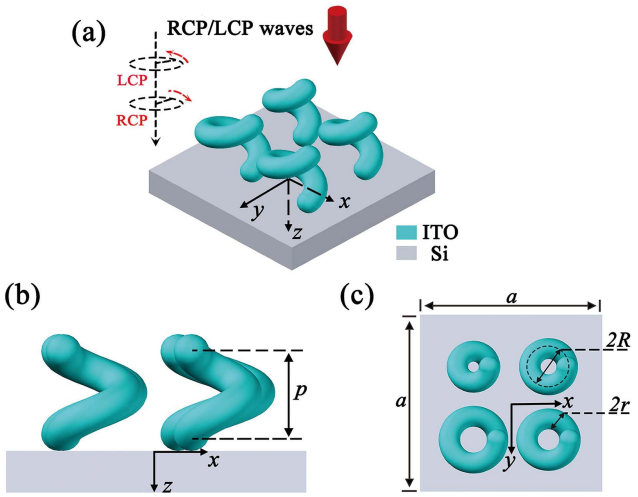

Fig. 1. Schematic diagrams of a chiral unit cell composed of four helices with different radii as subunits.

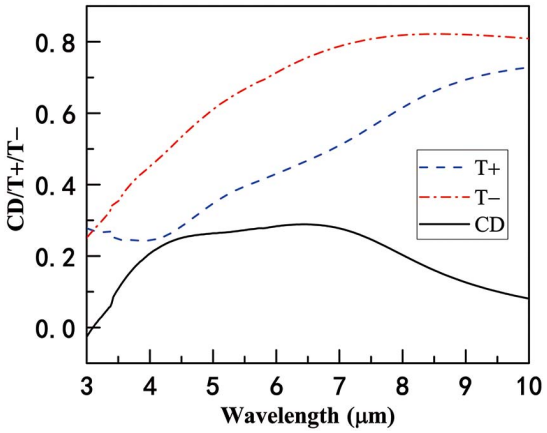

Fig. 2. CD and transmittances of the structure for the RCP and LCP incident waves.

manufactured by laser direct writing similar to the production processes in Refs. [33,38,39]. The process goes through four steps: coating photoresist, laser direct writing to form helix air gaps with different radii, depositing ITO in the helix air gaps, and removing photoresist.

A finite-difference time-domain (FDTD) method software was employed to simulate chiral properties of the structure. Due to the periodicity of the structure, we therefore considered a single unit cell with periodic boundary conditions in both x and y directions in simulations. It is assumed that a right-handed circularly polarized (RCP) wave and a left-handed circularly polarized (LCP) wave are incident along the z direction, respectively. In addition, perfect matched layer (PML) boundary conditions are set in the z direction. The permittivity of the silicon substrate is derived from experimental data[40], and the permittivity of ITO is determined by the Drude–Lorentz model[37].

3. Simulation Results and Discussion

By FDTD simulations, the transmission spectra of RCP and LCP waves were calculated and substituted into the CD formula below:

$$CD = |T_+ - T_-|, \tag{1}$$

where T_+, T_- are the transmittances for the RCP and LCP incident waves, respectively. The resulting CD spectrum at 3–10 μm was obtained, as shown in Fig. 2. From this figure, we can see that evident differences exist between T_+ and T_- in this band, leading to an obvious CD response of the structure. At about the wavelength of 6.44 μm, the value of CD reaches a maximum of 0.298. If the full width at half-maximum (FWHM) of CD is defined as such a wavelength range in which the CD drops to half of the maximum value, the FWHM is 5.06 μm ranging from 3.65 μm to 8.71 μm. The transmittance for the LCP wave is greater than that for the RCP wave in the 3.1–10 μm band. The reason is that the handedness of the circular polarization electromagnetic wave is identical to that of the helices of the structure. The selected model is a right-handed helix structure. When the RCP wave is incident, the helix structure composed of the ITO plasmonic material has a strong plasmon resonance, and the oscillation absorption is enhanced. In contrast, when the LCP wave is incident, the helix structure has a weak plasmon resonance due to their different handedness, and therefore the absorption is also weak.

We also simulated the distributions of electric field intensities in different cross sections vertical to the incident direction for the RCP and LCP waves at the wavelength of 6.44 μm, which is shown in Fig. 3. The cross sections were selected at 0.2 μm intervals from the incident end to the exit end. It can be seen from the figure that the field intensity at the upper end of the structure for the RCP wave incidence is the strongest, the plasmon resonance in ITO is also the strongest, and the field intensity gradually decreases from top to bottom. However, for the LCP wave incidence, the field intensity as well as the plasmon resonance is the strongest in the middle of the structure, and the plasmon resonances at the two ends weaken. These fields occur mainly on the surfaces of the helices, indicating that surface plasmon polaritons (SPPs) are induced. The couplings of the SPPs between different helices also appear, inflencing the CD responses of structures. By comparing them, the plasmon resonance caused by the RCP wave is stronger than the one for the LCP wave incidence. Therefore, the structure absorbs the RCP wave more strongly than the LCP wave, resulting in an obvious CD response. This is the same as the results shown in Fig. 2.

It is assumed that the structure is illuminated by a plane wave propagating in the positive z direction,

$$\vec{E}_i(\vec{r}, t) = \begin{pmatrix} i_x \\ i_y \end{pmatrix} e^{i(kz-\omega t)}, \tag{2}$$

where ω is the frequency, $k = \omega/c\sqrt{\varepsilon(\omega)}$ is the wave vector, and the complex amplitudes i_x and i_y describe the state of polarization. The transmitted field is then given by

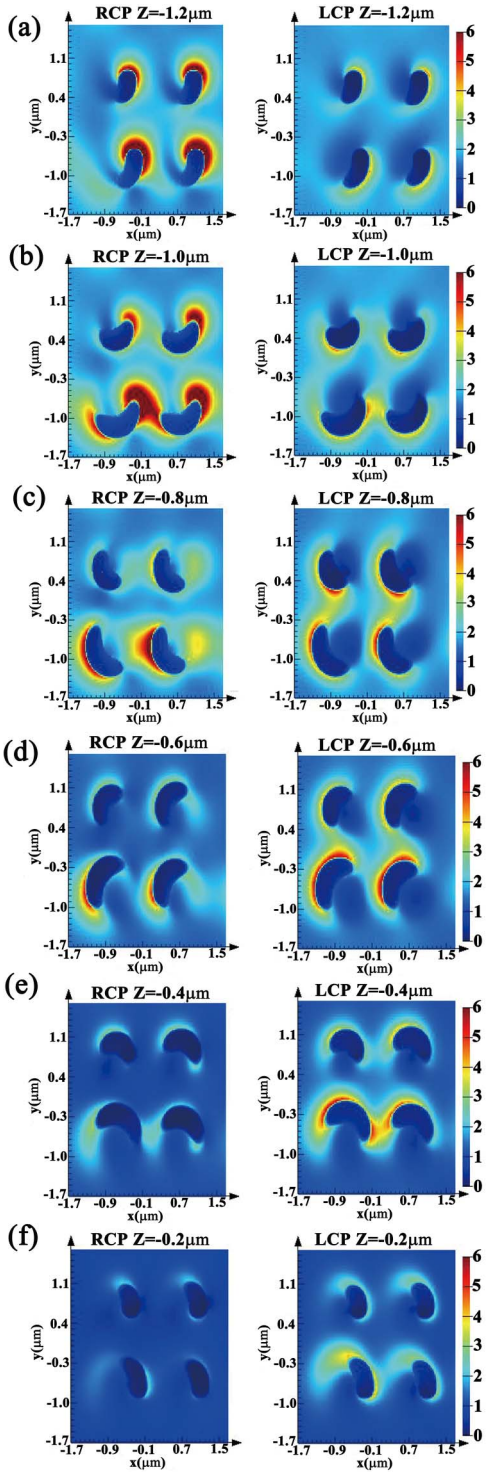

Fig. 3. Distributions of electric field intensities at different cross sections vertical to the incident direction under the RCP and LCP waves at the wavelength of 6.44 μm. (a) $z = -1.2$ μm; (b) $z = -1.0$ μm; (c) $z = -0.8$ μm; (d) $z = -0.6$ μm; (e) $z = -0.4$ μm; (f) $z = -0.2$ μm.

$$\vec{E}_t(\vec{r},t) = \begin{pmatrix} t_x \\ t_y \end{pmatrix} e^{i(kz-\omega t)}. \tag{3}$$

A complex Jones matrix T connects the generally complex amplitudes of the incident and the transmitted fields:

$$\begin{pmatrix} t_x \\ t_y \end{pmatrix} = \begin{pmatrix} T_{xx} & T_{xy} \\ T_{yx} & T_{yy} \end{pmatrix} \begin{pmatrix} i_x \\ i_y \end{pmatrix} = \begin{pmatrix} A & B \\ C & D \end{pmatrix} \begin{pmatrix} i_x \\ i_y \end{pmatrix} = T \begin{pmatrix} i_x \\ i_y \end{pmatrix}. \tag{4}$$

For circular states, the T matrix is given by[41]

$$T_{\text{circ}} = \begin{pmatrix} T_{++} & T_{+-} \\ T_{-+} & T_{--} \end{pmatrix} = \frac{1}{2} \begin{pmatrix} A + D + i(B - C) & A - D - i(B + C) \\ A - D + i(B + C) & A + D - i(B - C) \end{pmatrix}, \tag{5}$$

connecting the amplitudes of circularly polarized incident and transmitted waves:

$$\begin{pmatrix} t_+ \\ t_- \end{pmatrix} = T_{\text{circ}} \begin{pmatrix} i_+ \\ i_- \end{pmatrix}, \tag{6}$$

where "+" and "−" denote RCP and LCP waves, respectively. A, B, C, and D are influenced by the parameters, shapes, and components of the structure. Additionally, the couplings between different helices also affect their values, leading to the changes of CD.

The unit cell of the model proposed is composed of four subunits with different helix radii. In order to compare easily, four subunits were simulated separately, and the period remained the same as that of the original unit cell. Each subunit is in the middle of the unit cell. Their CD curves are shown in Fig. 4. The chirality of metamaterial structures usually occurs near the resonance frequencies of the structures. The resonance frequencies are closely related to the sizes of the structures. From this figure, it can be seen that for one of the subunits, corresponding resonance frequencies exist. With the increasing radius of the helix, the resonance of the subunit shifts towards the longer wavelengths. Their CD bandwidths are all narrower than that of the unit cell. The reason lies in that the unit cell is composed of four subunits with different helix sizes. Multiple resonance peaks caused by different subunits work together, leading to CD broadening.

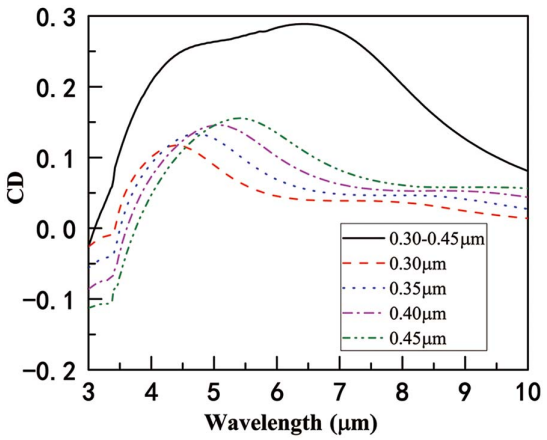

Fig. 4. CD curves of the original structure and single helix structures with radii of 0.30 μm, 0.35 μm, 0.40 μm, and 0.45 μm, respectively.

We change the number of turns of each subunit helix to keep them different. The simulated CD curves for two different cases are shown in Fig. 5, in which the original CD curve for the one turn helix is also plotted. Case one: the number of turns of the helix with the smallest radius is set to 1.07, the number of turns of the helix with the largest radius is set to 0.93, and those of the other two subunits remain at one. Case two: the number of turns of the helix with the second smallest radius is set to 1.04, and other parameters are the same as those of case one. It is found that for the adjusted structure, their CD values from 4.5 μm to 7 μm change between 0.265 and 0.274, while the CD values for the same number of turns change between 0.251 and 0.288. It means that the CD distributions with the adjusted structure are flatter, which provides a design idea for the flat-topped broadband CD.

To investigate the influences of structural materials on CD responses, we change the component of helices and replace ITO with Au and Ag. The other parameters remain unchanged. The dielectric constants of Au and Ag come from experimental data[40]. The simulated CD results are shown in Fig. 6. From this figure, we can see that the CD curves of the two material structures oscillate more than that of the ITO structure, which leads to narrower CD bandwidths. Therefore, to obtain the broadband CD responses in the mid-infrared band, ITO as a component is more advantageous. The figure also shows that the CD curves for the Au and Ag components are almost coincident. The reason is that their dielectric constants have slight changes in the band, leading to almost the same plasmon resonance behaviors.

Optical activity refers to the rotation ability of a polarized wave passing through the chiral structure, which can be expressed as

$$\theta = \frac{1}{2}[\arg(t_L) - \arg(t_R)], \tag{7}$$

where t_R and t_L stand for the transmission coefficients of RCP and LCP waves, respectively. Utilizing Eq. (7), we calculated optical activity corresponding to ITO, Ag, and Au structures with geometric parameters the same as those in Fig. 1. The results are shown in Fig. 7. For the ITO structure, its optical activity θ varies between 85° and 95° in the range of 4.5–10 μm. For the metallic (Ag and Au) structures, however, the optical activity shows strong oscillation with the change of wavelength. That is to say, the ITO helix structure shows relatively stable optical activity in the mid-infrared band, which provides a new idea for the design of mid-infrared broadband rotatory devices.

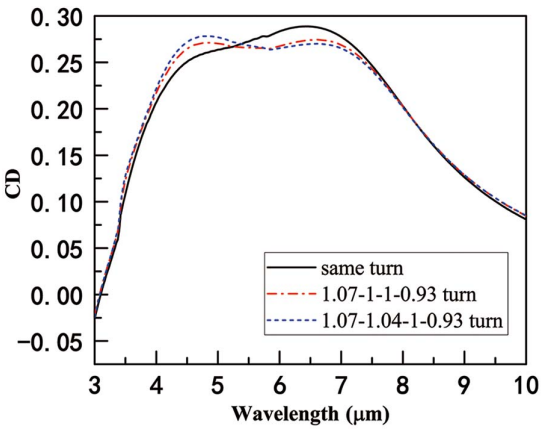

Fig. 5. CD properties of the structure with the different number of turns of subunits.

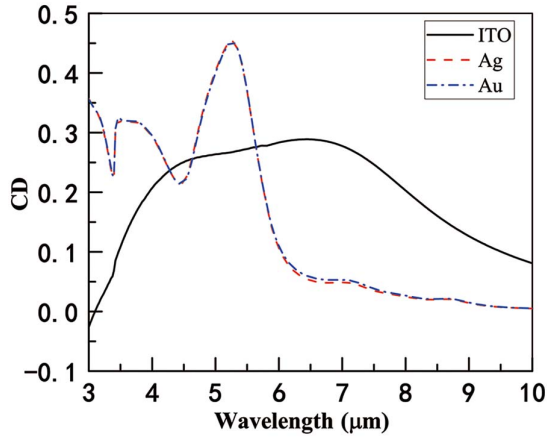

Fig. 6. CD properties of the original structure and structures with different components consisting of Ag and Au.

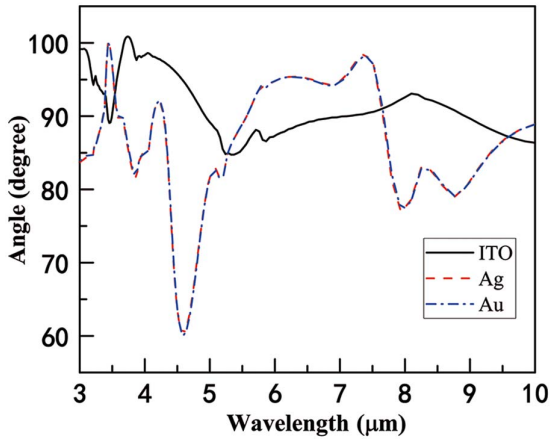

Fig. 7. Optical activity distributions of the structures with different components consisting of ITO, Ag, and Au, respectively.

4. Conclusion

In this paper, we proposed a periodic chiral structure, in which each unit cell consisting of four ITO helix subunits with different radii realized flat-topped broadband CD and optical activity in the mid-infrared band. The simulation results show that by optimizing parameters of the helix structure, flat-topped broadband CD distributions with their values from 4.5 μm to 7 μm can be obtained. The comparisons between the ITO helix structures and metallic (Ag and Au) helix structures show that the CD

and the optical activity of the former have broader bands, which provides a new idea for the design of broadband polarization state control devices in the mid-infrared band. Future work will be to further research the mechanism of chirality and explore improvement to the design of broadband chiral devices.

Acknowledgement

This work was supported by the National Natural Science Foundation of China (Nos. 61771227 and 62071208) and the Priority Academic Program Development of Jiangsu Higher Education Institutions (PAPD).

References

1. N. M. Estakhri, B. Edwards, and N. Engheta, "Inverse-designed metastructures that solve equations," Science **363**, 1333 (2019).
2. L. L. Spada and L. Vegni, "Near-zero-index wires," Opt. Express **25**, 23699 (2017).
3. J. Y. Xiao, R. W. Xiao, R. X. Zhang, Z. X. Shen, W. Hu, L. Wang, and Y. Q. Lu, "Tunable terahertz absorber based on transparent and flexible metamaterial," Chin. Opt. Lett. **18**, 092403 (2020).
4. N. J. Greybush, V. Pacheco-Peña, N. Engheta, C. B. Murray, and C. R. Kagan, "Plasmonic optical and chiroptical response of self-assembled Au nanorod equilateral trimers," ACS Nano **13**, 3875 (2019).
5. H. A. Atwater, "The promise of plasmonics," Sci. Am. **296**, 56 (2007).
6. F. Mattioli, G. Mazzeo, G. Longhi, S. Abbate, G. Pellegrini, E. Mogni, M. Celebrano, M. Finazzi, L. Duo, C. G. Zanchi, M. Tommasini, M. Pea, S. Cibella, R. Polito, F. Sciortino, L. Baldassarre, A. Nucara, M. Ortolani, and P. Biagioni, "Plasmonic superchiral lattice resonances in the mid-infrared," ACS Photon. **7**, 2676 (2020).
7. I. H. Lee, D. Yoo, P. Avouris, T. Low, and S. H. Oh, "Graphene acoustic plasmon resonator for ultrasensitive infrared spectroscopy," Nat. Nanotechnol. **14**, 313 (2019).
8. K. S. Novoselov, A. K. Geim, S. V. Morozov, D. Jiang, Y. Zhang, S. V. Dubonos, I. V. Grigorieva, and A. A. Firsov, "Electric field effect in atomically thin carbon films," Science **306**, 666 (2004).
9. J. H. Hu, J. Fu, X. H. Liu, D. P. Ren, J. J. Zhao, and Y. Q. Huang, "Perfect absorption in a monolayer graphene at the near-infrared using a compound waveguide grating by robust critical coupling," Chin. Opt. Lett. **17**, 010501 (2019).
10. L. L. Spada, C. Spooner, S. Haq, and Y. Hao, "Curvilinear meta surfaces for surface wave manipulation," Sci. Rep. **9**, 3107 (2019).
11. N. Meinzer, W. L. Barnes, and I. R. Hooper, "Plasmonic meta-atoms and metasurfaces," Nat. Photonics **8**, 889 (2014).
12. A. Kuzyk, R. Schreiber, Z. Y. Fan, G. Pardatscher, E.-M. Roller, A. Hogele, C. Friedrich, F. C. Simmel, A. O. Govorov, and T. Liedl, "DNA-based self-assembly of chiral plasmonic nanostructures with tailored optical response," Nature **483**, 311 (2012).
13. Z. Lalegani, S. A. S. Ebrahimi, B. Hamawandi, L. L. Spada, and M. S. Topark, "Modeling, design, and synthesis of gram-scale monodispersed silver nanoparticles using microwave-assisted polyol process for metamaterial applications," Opt. Mater. **108**, 110381 (2020).
14. R. Knipper, V. Kopecký, U. Huebner, J. Popp, and T. G. Mayerhöfer, "Slit-enhanced chiral- and broadband infrared ultra-sensing," ACS Photon. **5**, 3238 (2018).
15. K. Tanaka, D. Arslan, S. Fasold, M. Steinert, J. Sautter, M. Falkner, T. Pertsch, M. Decker, and I. Staude, "Chiral bilayer all-dielectric metasurfaces," ACS Nano **14**, 15926 (2020).
16. K. Höflich, T. Feichtner, E. Hansjürgen, C. Haverkamp, H. Kollmann, C. Lienau, and M. Silies, "Resonant behavior of a single plasmonic helix," Optica **6**, 1098 (2019).
17. C. He, T. Sun, J. J. Guo, M. Cao, J. Xia, J. P. Hu, Y. Yan, and C. H. Wang, "Metalens of circular polarization dichroism with helical surface arrays in mid-infrared region," Adv. Opt. Mater. **7**, 1901129 (2019).
18. L. K. Khorashad, L. V. Besteiro, M. A. Correa-Duarte, S. Burger, Z. M. Wang, and A. O. Govorov, "Hot electrons generated in chiral plasmonic nanocrystals as a mechanism for surface photochemistry and chiral growth," J. Am. Chem. Soc. **142**, 4193 (2020).
19. S. Droulias and L. Bougas, "Surface plasmon platform for angle-resolved chiral sensing," ACS Photon. **6**, 1485 (2019).
20. J. Kaschke, M. Blome, S. Burger, and M. Wegener, "Tapered *N*-helical metamaterials with three-fold rotational symmetryas improved circular polarizers," Opt. Express **22**, 19936 (2014).
21. J. Zhang, R. Tu, C. Huang, X. L. Yao, X. Hu, H. X. Ge, and X. F. Zhang, "Chiral plasmonic nanostructure of twistedly stacked nanogaps," Chin. Opt. Lett. **19**, 013601 (2021).
22. A. V. Rogacheva, V. A. Fedotov, A. S. Schwanecke, and N. I. Zheludev, "Giant gyrotropy due to electromagnetic-field coupling in a bilayered chiral structure," Phy. Rev. Lett. **97**, 177401 (2006).
23. S. Zhang, Y. S. Park, J. Li, X. Li, W. Zhang, and X. Zhang, "Negative refractive index in chiral metamaterials," Phys. Rev. Lett. **102**, 023901 (2009).
24. Y. Fang, R. Verre, L. Shao, P. Nordlander, and M. Käll, "Hot electron generation and cathodoluminescence nanoscopy of chiral split ring resonators," Nano Lett. **16**, 5183 (2016).
25. T. Fu, Y. Qu, T. Wang, G. Wang, Y. Wang, H. Li, J. Li, L. Wang, and Z. Zhang, "Tunable chiroptical response of chiral plasmonic nanostructures fabricated with chiral templates through oblique angle deposition," J. Phys. Chem. C **121**, 1299 (2017).
26. Y. Z. He, G. K. Larsen, W. Ingram, and Y. P. Zhao, "Tunable three-dimensional helically stacked plasmonic layers on nanosphere monolayers," Nano Lett. **14**, 1976 (2014).
27. Y. Z. He, K. Lawrence, W. Ingram, and Y. P. Zhao, "Strong local chiroptical response in racemic patchy silver films: enabling a large-area chiroptical device," ACS Photon. **2**, 1246 (2015).
28. R. Kolkowski, L. Petti, M. Rippa, C. Lafargue, and J. Zyss, "Octupolar plasmonic meta-molecules for nonlinear chiral watermarking at subwavelength scale," ACS Photon. **2**, 899 (2015).
29. V. E. Bochenkov and D. S. Sutherland, "Chiral plasmonic nanocrescents: large-area fabrication and optical properties," Opt. Express **26**, 27101 (2018).
30. A. G. Mark, J. G. Gibbs, T. C. Lee, and P. Fischer, "Hybrid nanocolloids with programmed three-dimensional shape and material composition," Nat. Mater. **12**, 802 (2013).
31. C. R. Han, L. C. Yang, P. Ye, E. P. J. Parrott, E. Pickwell-Macpherson, and W. Y. Tam, "Three dimensional chiral plasmon rulers based on silver nanorod trimers," Opt. Express **26**, 10315 (2018).
32. E. S. A. Goerlitzer, R. Mohammadi, S. Nechayev, P. Banzer, and N. Vogel, "Large-area 3D plasmonic crescents with tunable chirality," Adv. Opt. Mater. **7**, 1801770 (2019).
33. J. K. Gansel, M. Thiel, M. S. Rill, M. Decker, K. Bade, V. Saile, G. V. Freymann, S. Linden, and M. Wegener, "Gold helix photonic metamaterial as broadband circular polarizer," Science **325**, 1513 (2009).
34. M. Schnell, P. Sarriugarte, T. Neuman, A. B. Khanikaev, and R. Hillenbrand, "Real-space mapping of the chiral near-field distributions in spiral antennas and planar metasurfaces," Nano Lett. **16**, 663 (2016).
35. S. J. Zhang, Y. Li, Z. P. Liu, J. L. Ren, Y. F. Xiao, H. Yang, and Q. Gong, "Two-photon polymerization of a three dimensional structure using beams with orbital angular momentum," Appl. Phy. Lett. **105**, 061101 (2014).
36. Y. L. Zhu, B. W. Cao, J. W. Li, Y. Wu, A. X. Lu, L. Y. Qian, C. Q. Han, and C. C. Yan, "L-shaped ITO structures fabricated by oblique angle deposition technique for mid-infrared circular dichroism," Opt. Express **27**, 33243 (2019).
37. G. V. Naik, V. M. Shalaev, and A. Boltasseva, "Alternative plasmonic materials: beyond gold and silver," Adv. Mater. **25**, 3264 (2013).
38. K. Gansel, M. Latzel, A. Frolich, J. Kaschke, M. Thiel, and M. Wegener, "Tapered gold-helix metamaterials as improved circular polarizers," Appl. Phy. Lett. **100**, 101109 (2012).
39. K. Johannes and M. Wegener, "Gold triple-helix mid-infrared metamaterial by STED-inspired laser lithography," Opt. Lett. **40**, 3986 (2015).
40. E. D. Palik, *Handbook of Optical Constants of Solids* (Academic, 1997).
41. C. Menzel, C. Rockstuhl, and F. Lederer, "Advanced Jones calculus for the classification of periodic metamaterials," Phys. Rev. A **82**, 053811 (2010).